Chin. J. Astron. Astrophys. Vol. 6 (2006), No. 1, 87–95
(*http://www.chjaa.org*)

Chinese Journal of
Astronomy and
Astrophysics

Three-dimensional Distribution of the Escape Photons of Hα Flares *

Ming-Guo Sun[1,3], Zhong-Quan Qu[1], Zhi Xu[2], Xiao-Yu Zhang[1], Cheng-Lin Xu[1,3], Shuai Wang[1,3] and Chun-Lan Jin[1,3]

[1] Yunnan Astronomical Observatory/National Astronomical Observatories, Chinese Academy of Sciences, Kunming 650011; *sunmg@ynao.ac.cn*
[2] Department of Astronomy, Nanjing University, Nanjing 210093
[3] Graduate University of the Chinese Academy of Sciences, Beijing 100049

Received 2004 July 22; accepted 2005 July 26

Abstract A technique for obtaining a three-dimensional distribution of received photons in Hα flares in the solar atmosphere is presented. It is well known that during flares hydrogen atoms in the chromosphere and photosphere are excited (even ionized) by the downward heating of non-thermal particles and then emit Hα photons. We trace back these Hα photons to their original layers by use of the contribution function in the theory of spectral line formation, and so acquire their three-dimensional (3D) distribution. This technique is applied to the two-ribbon flare of 2002 January 20. The atmospheric models are obtained by fitting the "quasi-profiles" with the help of the generally used model atmospheres. Since the variety of the 3D images reflects the response of the atmospheric layers to the impact of energy transport, an analysis of the development of the flare is given through a comparison of the 3D images with the 2D temperature distribution.

Key words: line: formation – radiative transfer – sun: flares

1 INTRODUCTION

Solar flares are widely believed to originate from magnetic reconnection in the corona. During a flare eruption a large amount of energy is transported downward by high-energy particles such as electrons, protons, and ions, etc., and by irradiation and heat conduction. This process has attracted many researchers in solar physics and many of its aspects have been explored, for instance, the energy budget, the mechanism of energy release, the acceleration of the electrons, protons and ions (Tandberg-Hanssen & Emslie 1988; Asai 2003), the non-thermal processes of these particles (especially by electrons) (Hudson 1972; Lin & Hudson 1976; Fang et al. 1993; Ding et al. 2002) and the heating mechanism of the lower atmosphere (Canfield & Gunkler 1984; Metcalf & Canfield et al. 1990). When the hydrogen atoms in the lower atmosphere are heated by the non-thermal particles they would emit Hα photons (Brown 1973; Emslie 1978), so the Hα line provides one of the best diagnostic tools for studying the mechanism of energy transport in the solar atmosphere.

The spectral line formation theory tells us that different lines and different wavelength points within the lines are formed in different layers of the atmosphere. The contribution function for a

* Supported by the National Natural Science Foundation of China.

line defines the contribution by different layers to the emergent specific intensity at the wavelengths within the line (Staude 1972) or the depth distribution of the escaping photons (Qu et al. 2002a, 2002b). It should be pointed out that much previous research work emphasizes the problems: which contribution function can be optimally used to obtain the height of the line formation (Magain 1986), or can be used for both the absorption and emission lines (Achmad et al. 1991).

According to quantum mechanics, if the received photons at every point in a given observed area are redistributed to the layers according to the contribution functions and the redistributed quanta of different wavelengths within the line are added to each layer, then a reconstructed 3D image is obtained (Qu et al. 2002a; Xu et al. 2002). The variety of the 3D images of escaping photons helps us to know the response of the lower atmosphere to the downward energy transport and the evolution of flares. We then obtain a model atmosphere by fitting the "quasi-profiles" drawn from the serial tuning filtering observations of the adjacent wavebands with the help of the generally used atmospheric models (Machado et al. 1980; Vernazza et al. 1981; Ding et al. 1994; Fang et al. 1995).

In this paper, we first outline the sampled flare, fit the observed profiles to obtain the atmospheric models which determine the contribution functions, and then present the 3D distribution images of escaping photons of the flare. Finally, conclusions and discussion are given by comparing the 3D images with the 2D temperature distributions.

2 OBSERVED FLARE, ATMOSPHERIC MODEL AND 2D DISTRIBUTION OF TEMPERATURE

In this section, we describe the observed flare and the drawing of flare patches. In order to avoid the center-to-limb variation, the observed objects are restricted to the vicinity of the center of the solar disk, and the atmosphere model is determined by fitting the "quasi-profiles". Finally we present the 2D distribution of the temperature of the flare at height 1204 km.

2.1 The Event

A C2.8-class two-ribbon Hα flare took place in AR9788 on 2002 January 20. It started at 23:07 UT and ended at about 00:20 UT. The Hα maximum intensity happened at about 23:11 UT. Figure 1 shows the development of the flare taken at the line center observed with the 40 cm telescope of the Big Bear Solar Observatory (BBSO). Figure 2 illustrates the line-center and off-line-center observations of the flare at 23:18 UT. One can notice some sunspots in this area in the bandpasses far off the line-center (≥ 0.75 Å and ≤ -0.75 Å). For the present study we select six time instants with observations covering the range -1.25 Å to $+1.25$ Å of the line-center at steps of 0.25 Å. The short line in the left-lower corner in the left-lower frame represents a distance of 5000 km.

2.2 Drawing of Flare Patches

We first plotted out the flaring areas in 14 contour levels of relative intensity from 4500 to 1900 at steps of 200 for six instants of time between 23:11 UT and 00:06 UT. We then obtain the line profile for each flaring point. The profiles are blurred slightly by the scanning time of about 35 seconds from –1.25 Å to +1.25 Å. However, such a distortion will cause negligible errors in the model calculations, hence in the reconstructed 3D images. We found that within each region surrounded by the contours the line profiles of all the points varied a little, this led us to fit typical profiles rather than all the profiles, using the standard model atmosphere or its modified form. We have a total of 14 such regions and the typical profiles are labelled as Profiles 101, 102, $\cdots$, 114 in decreasing order of the peak at the line center. These 14 profiles are marked with the $*$, $+$ and $\triangle$ lines in Figure 3 . For convenience we use one model for each zone. In the next section we will illustrate with one particular zone. Figure 3 shows that the profile center declines after the flaring phase. This phenomenon was especially analyzed by some authors (Canfield & Gayley 1987; Ding 2003; Berlicki et al. 2004).

At the first time instant, the flare took on the form of five bright dots. These then spread out, and some of them joined up to form ribbons, which became wider and wider as the flare developed.

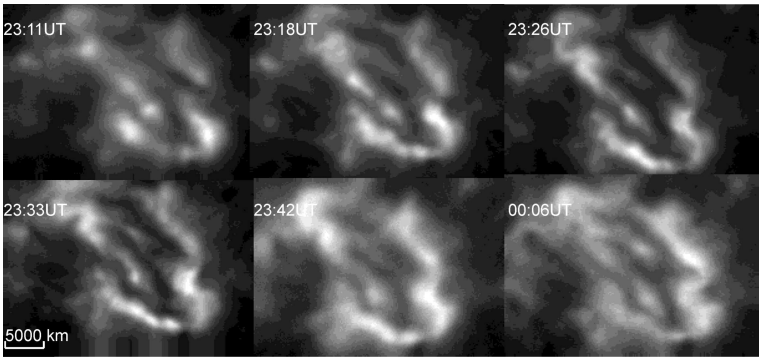

Fig. 1 Development of the Hα flare on 2002 January 20, as shown by the line center filtered observation.

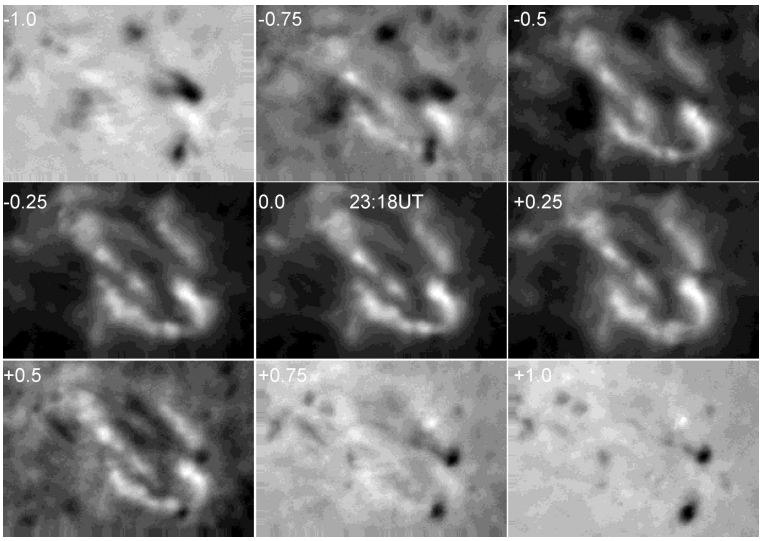

Fig. 2 Line-center and off-line-center observations of the flare. The number in each frame indicates the distance between the bandpass center and the line center in units of Å.

It is readily seen that not all the spatial points are heated in unison. For example, the central dot disappeared before the flare maximum.

2.3 Atmospheric Models and Fitting

The main process of constructing the model atmosphere is described as follows : The column mass density (m), temperature (T), electron number density (n_e) and the micro-turbulent velocity (v_t) were acquired by interpolation of the flare models F1 and F2 (Machado et al. 1980), of the quiet sun model of VAL3c (Vernazza et al. 1981) and of the white-light flare model (Ding et al. 1994; Fang et al. 1995). T, n_e and v_t are taken to be functions of m that satisfy the hydrostatic equilibrium condition $p =$mg, where $p = ((1 + \alpha_{\rm H_e})n_{\rm H}+n_e){\rm kT} + \frac{1}{2}\rho {v_t}^2$, the relative abundance of helium was taken as $\alpha_{\rm H_e} = 0.1$, and the acceleration of gravity, $g = 2.74 \times 10^4$ cm s^{-2}.

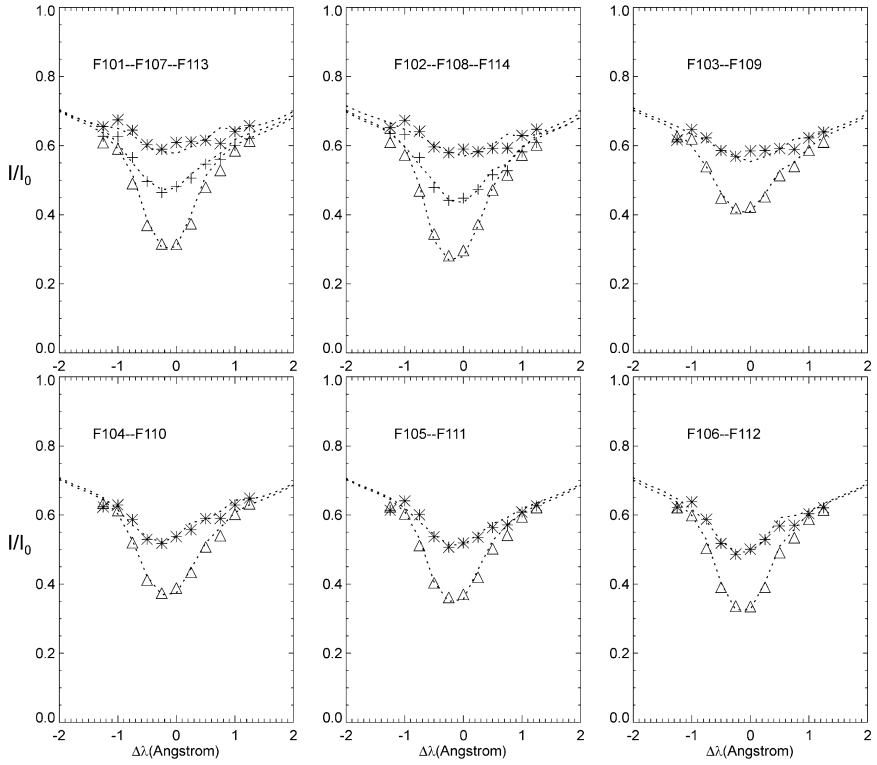

Fig. 3 Observed Hα profiles (asterisks and triangles) and fit profiles (dotted lines).

A plane-parallel atmosphere was assumed, and the computing code (Multi v2.2) was used to solve the multi-level non-LTE problems in the moving atmospheres (Carlsson 1986). The code proposed by Ding & Fang (1989) was also used to compute the line parameters at 151 points equally spaced along the line of sight. Liu et al. (2002) considered v_t as one of the main causes of the line broadening. By trial and error, we adjusted T and v_t, and repeated the computation until the computed profiles reached a good match with the observed ones. Finally, we obtain the model-fits to the 14 observed profiles F101–F114. Figure 3 shows the results of fitting the H_α profiles. Table 1 lists the numerical data of F114. Figure 4 shows the temperature profiles of F101 and F114. For 23:11 UT, we used the eight models F101–F108; for 23:18 UT, the six models F105–F110; for 23:26 UT, the eight models F104–F111; for 23:33 UT, the six models F107–F112; for 23:42 UT, the three models F111–F113; for 00:06 UT, the three models of F112–F114. Although the magnetic field plays an important role in solar activities (Falchi et al. 1990), it is not taken into account in the atmospheric models as the H_α line is not particularly sensitive to it.

2.4 2D Distribution of Temperature

After determining the model atmosphere, we obtain the temperature for every point of the flare, then we work out the two-dimensional (2D) temperature distribution of the flare at height 1204 km for the six selected times (see Fig. 5). The background is arbitrarily assumed to be the VAL model atmosphere (Vernazza et al. 1981), with a temperature of about 6300 K. In the first several minutes, especially during the impulsive phase the chromosphere was heated quickly (Gan et al. 1987). At 23:11 UT the flare had reached its maximum temperature. Comparing Figure 5 with Figure 1 we can find that it became brighter in Hα just as it was cooling down (Ding 2003).

Table 1 Model F114, $m_0 = 3.94 \times 10^{-4}$g cm^{-2}

h (km)	$m - m_0$ (g cm^{-2})	T (K)	v_t (km s^{-1})	n_e (cm^{-3})	$n_{\rm H}$ (cm^{-3})	b_1	b_2	b_3
1448	3.832E–06	447000	7.02	6.885E+10	1.658E+04	1.187E+06	9.257E+00	1.118E+00
1429	4.548E–06	141000	7.00	2.165E+11	8.163E+05	4.856E+05	7.713E+00	1.105E+00
1426	4.749E–06	112000	6.36	2.718E+11	2.081E+06	4.140E+05	8.098E+00	1.129E+00
1423	5.016E–06	70000	6.34	4.315E+11	1.809E+07	3.025E+05	1.044E+01	1.237E+00
1422	5.301E–06	32000	6.32	9.227E+11	2.101E+09	1.642E+05	4.159E+01	2.177E+00
1421	5.448E–06	26000	6.31	1.122E+12	1.033E+10	1.284E+05	7.221E+01	2.922E+00
1420	6.000E–06	18000	6.29	1.554E+12	1.777E+11	4.408E+04	1.038E+02	3.150E+00
1419	6.249E–06	15000	6.28	1.801E+12	5.704E+11	1.388E+04	7.214E+01	2.300E+00
1418	6.931E–06	9000	6.24	2.236E+12	3.422E+12	2.348E+01	7.394E+00	5.126E–01
1414	1.240E–05	8466	6.13	1.956E+12	4.437E+12	1.063E+01	6.300E+00	7.212E–01
1401	3.007E–05	8390	6.01	1.621E+12	4.503E+12	7.623E+00	5.922E+00	1.026E+00
1395	3.898E–05	8343	6.01	1.552E+12	4.595E+12	6.660E+00	5.708E+00	1.073E+00
1302	9.886E–05	8211	9.47	1.247E+12	3.844E+12	5.152E+00	5.178E+00	1.342E+00
1291	1.138E–04	8185	8.38	1.211E+12	4.469E+12	4.663E+00	4.710E+00	1.296E+00
1272	1.446E–04	8128	6.01	1.189E+12	6.104E+12	3.858E+00	3.926E+00	1.157E+00
1254	1.795E–04	8061	4.23	1.216E+12	7.773E+12	3.282E+00	3.364E+00	1.038E+00
1240	2.165E–04	8003	2.47	1.240E+12	9.495E+12	2.896E+00	2.960E+00	9.417E–01
1225	2.571E–04	7950	2.24	1.262E+12	1.056E+13	2.659E+00	2.712E+00	8.831E–01
1211	3.020E–04	7900	2.02	1.283E+12	1.174E+13	2.462E+00	2.497E+00	8.294E–01
1204	3.258E–04	7869	1.98	1.281E+12	1.236E+13	2.356E+00	2.392E+00	8.038E–01
1190	3.761E–04	7796	1.96	1.258E+12	1.372E+13	2.146E+00	2.188E+00	7.547E–01
1182	4.041E–04	7760	1.95	1.246E+12	1.447E+13	2.053E+00	2.093E+00	7.313E–01
1168	4.619E–04	7693	1.93	1.224E+12	1.602E+13	1.896E+00	1.933E+00	6.916E–01
1153	5.270E–04	7626	1.83	1.204E+12	1.782E+13	1.759E+00	1.793E+00	6.569E–01
1139	5.972E–04	7563	1.81	1.184E+12	1.970E+13	1.647E+00	1.678E+00	6.288E–01
1124	6.753E–04	7501	1.78	1.165E+12	2.180E+13	1.551E+00	1.579E+00	6.051E–01
1087	9.118E–04	7320	1.75	1.053E+12	2.835E+13	1.345E+00	1.370E+00	5.612E–01
1024	1.470E–03	7020	1.72	8.726E+11	4.407E+13	1.149E+00	1.172E+00	5.409E–01
961	2.325E–03	6726	1.68	6.526E+11	6.879E+13	1.060E+00	1.084E+00	5.694E–01
897	3.684E–03	6460	1.66	5.173E+11	1.089E+14	1.023E+00	1.050E+00	6.271E–01
832	5.849E–03	6220	1.63	4.347E+11	1.744E+14	1.009E+00	1.037E+00	7.013E–01
766	9.374E–03	6033	1.61	4.061E+11	2.822E+14	1.004E+00	1.030E+00	7.702E–01
700	1.516E–02	5833	1.55	3.807E+11	4.665E+14	1.001E+00	1.021E+00	8.570E–01
635	2.474E–02	5620	1.52	3.582E+11	7.836E+14	1.000E+00	1.011E+00	9.671E–01
568	4.152E–02	5393	1.49	3.700E+11	1.363E+15	1.000E+00	9.979E–01	1.110E+00
501	7.074E–02	5190	1.46	4.307E+11	2.404E+15	1.000E+00	9.875E–01	1.268E+00
455	1.046E–01	5010	0.93	5.649E+11	3.744E+15	1.000E+00	9.811E–01	1.446E+00
395	1.755E–01	4896	0.91	8.723E+11	6.419E+15	1.000E+00	9.834E–01	1.578E+00
351	2.602E–01	4830	0.90	1.186E+12	9.641E+15	1.000E+00	9.867E–01	1.660E+00
338	2.900E–01	4820	0.90	1.298E+12	1.077E+16	1.000E+00	9.877E–01	1.671E+00
326	3.231E–01	4855	0.80	1.436E+12	1.194E+16	1.000E+00	9.894E–01	1.614E+00
314	3.600E–01	4890	0.80	1.588E+12	1.321E+16	1.000E+00	9.909E–01	1.557E+00
273	5.122E–01	4943	0.91	2.215E+12	1.853E+16	1.000E+00	9.940E–01	1.455E+00
232	7.287E–01	4996	0.92	3.090E+12	2.607E+16	1.000E+00	9.963E–01	1.353E+00
191	1.037E+00	5050	0.93	4.311E+12	3.670E+16	1.000E+00	9.976E–01	1.269E+00
147	1.490E+00	5150	1.23	6.142E+12	5.124E+16	1.000E+00	9.987E–01	1.182E+00
98	2.204E+00	5410	1.41	1.001E+13	7.173E+16	1.000E+00	9.997E–01	1.070E+00
49	3.186E+00	5790	1.56	1.977E+13	9.648E+16	1.000E+00	1.000E+00	1.012E+00
20	3.911E+00	6180	1.62	4.052E+13	1.109E+17	1.000E+00	1.000E+00	9.849E–01
0	4.444E+00	6520	1.89	7.676E+13	1.183E+17	1.000E+00	1.000E+00	9.914E–01
–9	4.726E+00	6720	1.93	1.104E+14	1.219E+17	1.000E+00	1.000E+00	9.967E–01
–28	5.306E+00	7280	2.15	2.798E+14	1.253E+17	1.000E+00	1.000E+00	9.983E–01
–48	5.903E+00	7900	2.26	6.897E+14	1.276E+17	1.000E+00	1.000E+00	9.998E–01
–68	6.511E+00	8540	2.38	1.540E+15	1.284E+17	1.000E+00	1.000E+00	1.000E+00

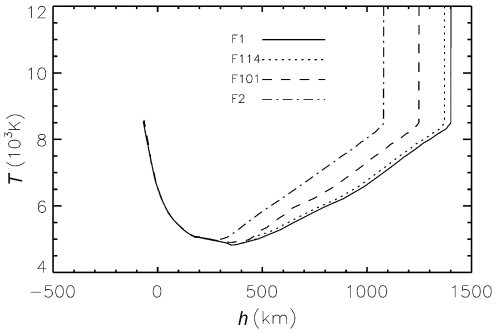

Fig. 4 Height profiles of temperature of the sample models F1, F101, F114 and F2.

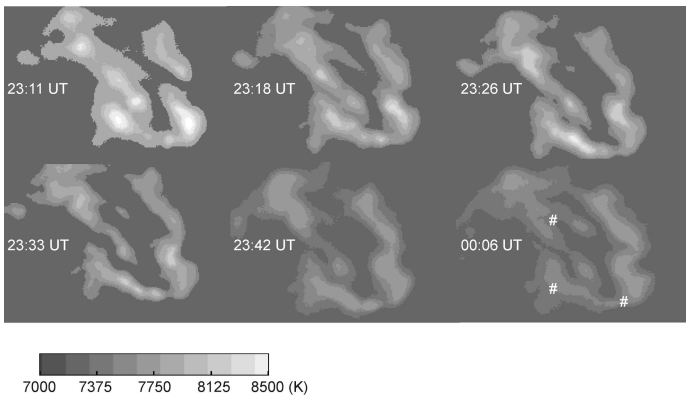

Fig. 5 Temperature distribution of the flare at height 1204 km at six time instants. The background is arbitrarily assumed to be the VAL model atmosphere.

3 CONTRIBUTION FUNCTION AND THE RECONSTRUCTION OF 3D IMAGES OF THE ESCAPING PHOTONS

Once the thermodynamic parameters were determined by the fitting, we calculated the contribution function, the formal contribution function that defines the depth distribution of the received photons and hence the configuration of the reconstructed 3D images.

3.1 Contribution Function

There are many choices for the function but different functions have different meanings (Magain 1988). Here, we adopt the one (Qu et al. 1999) which can indicate the distribution of the received photons, and was derived from the following formal solution to the radiative transfer equation:

$$I_\nu(0) = \sum_{i=1}^{n} CF(\lambda, h_i), \tag{1}$$

where $I_\nu(0)$ is the emergent specific intensity at the wavelength λ, and the contribution function CF_i to the first-order derivative term is

$$CF(\lambda, h_k) = e^{-\tau_{k-1}}\Big[(1 - e^{-\triangle\tau_{k-1}})S_t(\tau_k) + (1 - e^{-\triangle\tau_{k-1}} - \triangle\tau_{k-1})\frac{dS_t(\tau_k)}{d\tau}\Big]. \tag{2}$$

In the above equation, S_t is the total source function and τ the total line-of-sight opacity, defined respectively as

$$S_t = \frac{\chi_c S_c + \chi_l \phi_\nu S_l}{\chi_c + \chi_l \phi_\nu} = \frac{r_0 S_c + \phi_\nu S_l}{r_0 + \phi_\nu}, \tag{3}$$

and

$$d\tau = -(\chi_c + \chi_l \phi_\nu) dz/\mu, \tag{4}$$

where χ_l is the line absorption coefficient, χ_c the continuum absorption coefficient and ϕ_ν the absorption profile, provided that the complete frequency redistribution stands. For the filtering observations, photons are received within the whole bandpass of the Hα line rather than a single wavelength point, and the used bandpass $\Delta\lambda_{bp} = 0.25$Å. Therefore, Eq. (2) should be integrated first:

$$CF_{bp}(\Delta\lambda_{bp}, h_i) = \int_{\lambda_{0,bp}-\frac{1}{2}\Delta\lambda_{bp}}^{\lambda_{0,bp}+\frac{1}{2}\Delta\lambda_{bp}} CF(\lambda, h_i) d\lambda \frac{1}{\Delta\lambda_{bp}}, \tag{5}$$

where $\lambda_{0,bp}$ is the central wavelength of the bandpass, and $h(= z/\mu)$ the slant geometric height along the line of sight. The normalized distribution describing the photon distribution from height grid h_i can be obtained by normalizing Eq. (5),

$$CF'_{bp}(\Delta\lambda_{bp}, h_i) = CF_{bp}(\Delta\lambda_{bp}, h_i) / \int_{h_n}^{h_0} CF_{bp}(\lambda, h) dh, \tag{6}$$

where h_n is the lowest height grid of the model atmosphere considered, and h_0 the highest one. It is worth noting that because the transfer equation describes the transfer of both emission and absorption, the normalized contribution function expresses the received photons which are emitted and escaped from the considered layers.

3.2 Reconstruction of 3D Image of the Escaping Photons

To view the development of the flare in three dimensions, a reconstruction of 3D images of the escaping photons of the flare was carried out (see Fig. 6). In the figure, h represents the geometric height measured along the line of sight. The scale is enlarged so the variation in the number of escaping photons can be seen more clearly. The other two axes define the plane perpendicular to the line of sight. The flare spreads over some 19 000 km in the west-east direction and 21 000 km north-south at maximum. The difference in number of the photons in different layers is suitably decreased in order to have a better representation.

As mentioned above, the 3D images give the distribution of escaping photons at each level along the line of sight and reflect the contribution of each level to the total emergent emission in the flare eruption. Furthermore, the escaping photons are produced because the atmosphere is heated or bombarded by the non-thermal particles. All the escaping photons resulted from the excitation of the corresponding emission. In Figure 6, the 3D images are plotted at an angle in order to show more clearly the depth distribution. However, this operation does not mean lateral radiative transfer. The most striking phenomenon in all of the six frames is the gap that separates the depth distribution into two regions (see fig. 1 of Vernazza et al. 1981). The gap covers the minimum temperature region of few escaping photons. We should state that we have taken out the background radiation. It is the result of the *CF* curves (see figs. 3 and 4 of Xu et al. 2002), which actually indicates that the heating and bombardment in this region can hardly cause hydrogen to emit H_α photons.

We have found that different parts of the flare do not develop in step. We can divide the flare region into four parts as shown in Figure 1 : left-upper, left-lower, right-upper and right-lower. At 23:42 UT, the right-upper part began to flare rapidly, while the left-lower one began to grow dim. Comparing it with the 2D images shown in Figure 5 we see that it became cooler due to the heat radiation. Finally, at 00:06 UT, the left-lower part, half of the left-upper and half of the

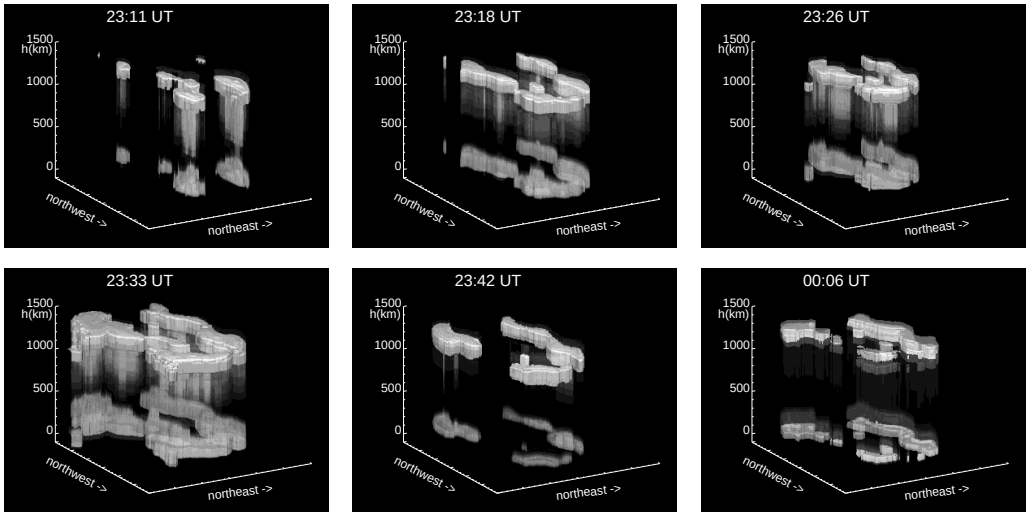

Fig. 6 3D distribution of escaping photons at six selected time instants in the flare of 2002 January 20. 'h' represents the geometric height measured along the line of sight, the other two axes determine the plane perpendicular to the line of sight and the minimum temperature region is located near height 500 km.

right-lower parts (these parts are marked with ♯ in Fig. 5) almost recovered the temperature of the quiet region, and their outlines faded away. In contrast, the right-upper part which did not erupt until 23:26 UT still had a high temperature. When this part turned into a quiet area, all flaring ceased.

4 CONCLUSIONS AND DISCUSSION

As pointed out above, the 3D images of the Hα escaping photons provide us with an intuitive picture of how energy is transported downward in the atmosphere following a magnetic reconnection. In this paper, as an example, we reconstruct a time sequence of 3D images of the H_α flare of 2002 Jan 20. When we compare the 3D images one by one with the temperature distribution, we find the following features : (1) At the first time instant (23:11 UT), the maximum temperature was already reached, while there were only some small flaring spots in the Hα image (see Figs. 1 and 6). This shows that the number of hydrogen atoms excited to second energy level was not so great in that region, partly due to the small plasma density or a too high temperature which would excite the hydrogen atoms to higher levels. As the temperature dropped, more and more Hα photons emerged and the number reached a maximum at 23:33 UT. Figure 5 shows that as the Hα radiation takes away the energy, the temperature drops. (2) The Hα photons came mainly from two regions (Vernazza et al. 1981), one in the chromosphere and one in the photosphere. However, a few Hα photons did emerge from the region in between. (3) Figure 4 shows that the temperature below the region of lowest temperature varied little, while Figure 6 shows that the amount of escaping Hα photons varied markedly. This indicates that non-thermal particles (e.g., electrons) may play a role in the excitation (and ionization) of the hydrogen atoms. (4) It is worth noting that this was a complicated two-ribbon flare, and its different parts and kernels did not develop in step. The development of the flare shown in the 3D images is consistent with the classical picture of chromospheric flares.

However, because of the limited precision of the "quasi-line" and the number of the atmospheric models, our results provide only an approximate indication to fact. When we gain more atmospheric

models, and thus more accurate $CF's$ to fit the spectra obtained with the telescope, the resulting 3D image will better reflect reality. This will be our future work.

Acknowledgements This work is supported by the National Natural Science Foundation of China (Grant No. 19773016) and the Grand Basic Development and Study Foundation of China (Grant No. 2000078401).We are grateful to the group of BBSO, especially to Prof. H.M.Wang, for giving us their generous support to obtain the observed data. Finally, we wish to thank Prof. M. D. Ding for useful discussions and constructive suggestions.

References

Achmad L., De Jager C., Nieuwenhuijzen H., 1991, A&A, 250, 450
Asai A., Ishii T., Kurokawa H. et al., 2003, ApJ, 586, 624
Berlicki A., Heinzel P., 2004, A&A, 420, 319
Brown J. C., 1973, Solar Physics, 31, 143
Canfield R. C., Gayley K. G., 1987, ApJ, 322, 999
Canfield R. C., Gunkler T. A., Ricchiazzi P. J., 1984, ApJ, 282, 296
Carlsson M., 1986, Uppsala Astronomical Observatory Report, 33
Ding M. D., 2003, Journal of The Korean Astronomical Society, 36, 49
Ding M. D., Fang C., 1989, A&A, 225, 204
Ding M. D., Fang C., Gan W. Q. et al., 1994, ApJ, 429, 890
Ding M. D., Qiu J., Wang H. M., 2002, ApJ, 576, 83
Emslie A. G., 1978, ApJ, 224, 241
Falchi A., Falciani R., Smaldone L. A., 1990, A&AS, 84, 601
Fang C., Henoux J. C., Gan W. Q., 1993, A&A, 274, 917
Fang C., Henoux J. C., Hu Ju et al., 1995, Solar Physics, 157, 271
Gan W. Q., Fang C., 1987, Solar Physics, 107, 311
Hudson H. S., 1972, Solar Physics, 24, 414
Lin R. P, Hudson H. S., 1976, Solar Physics, 24, 414
Liu Y., Ding M. D., 2002, ChJAA, 2(3), 277
Magain P., 1986, A&A, 163, 135
Metcalf T. R., Canfield R. C., Saba J. L. R., 1990, ApJ, 365, 391
Machado M. E., Avrett E. H., Vernazza J. E. et al., 1980, ApJ, 242, 336
Qu Z. Q., Jiang Y. C., Luan T. et al., 2002a, ASP Conference Series, 200, 303
Qu Z. Q., Xu Z., 2002b, ChJAA, 2(1), 71
Qu Z. Q., Zhang X. Y., Xu Z., 2001, ChJAA, 1(2), 161
Qu Z. Q., Zhang X. Y., Gu X. M., 1999, MNRAS, 305, 737
Staude J., 1972, Solar Physics, 24, 255
Tandberg-Hanssen E., Emslie A. G., 1988, The Physics of Solar Flares, Cambridge University Press
Vernazza J. E., Avertt E. H., Loeser R., 1981, ApJS, 45, 635
Xu Z., Qu Z. Q., Zhang X. Y. et al., 2002, Science in China (Series A), 45 Supp., 51